Conformational change of an amylose derivative in chiral solvents: Amylose tris(*n*-butylcarbamate) in ethyl lactates

Shota Arakawa,[a] Ken Terao,*[a] Shinichi Kitamura[b] and Takahiro Sato[a]

[a] *Department of Macromolecular Science, Osaka University, 1-1 Machikaneyama-cho, Toyonaka, Osaka 560-0043, Japan. Fax: +81-6-6850-5461; Tel: +81-6-6850-5459; E-mail: kterao@chem.sci.osaka-u.ac.jp*

[b] *Graduate School of Life and Environmental Sciences, Osaka Prefecture University, Gakuen-cho, Nakaku, Sakai, Osaka 599-8531, Japan*

†Electronic Supplementary Information (ESI) available: Concentration dependence of the scattering intensity, supplementary explanations for the two-state wormlike chain model and the lattice model. See DOI: 10.1039/b000000x/

The *z*-average radius of gyration, the particle scattering function and the intrinsic viscosity have been determined for amylose tris(*n*-butylcarbamate) (ATBC) in $_{D}$-, $_{DL}$- and $_{L}$-ethyl lactates all at 25 °C by light and small-angle X-ray scattering and viscometry as functions of the weight-average molecular weight in a range from 1.7×10^4 to 1.7×10^6 to investigate the chiral solvent dependence of the helical conformation of the amylose derivative. The data were analyzed in terms of the wormlike chain model to determine the Kuhn segment length λ^{-1} (the stiffness parameter) and the helix pitch per residue h. The λ^{-1} value of 49 nm in $_{D}$-EL is 52 % larger than 32 nm in $_{L}$-ethyl lactate, an unmistakable chiral solvent effect to the helical conformation of the amylose derivative, and the relation between h and λ^{-1} is consistent with that obtained previously in nine different solvents [*Polymer*, 2010, **51**, 4243]. The content of intramolecularly hydrogen bonding C=O groups in $_{D}$-ethyl lactate is estimated to be 15 % more than that in $_{L}$-ethyl lactate, confirmed by heats of dilution for ethyl lactate solutions of ATBC estimated by isothermal titration calorimetry.

Introduction

Amylose and cellulose carbamates are known to be typical semiflexible polymers[1] and widely used in enantioseparation chromatography as the chiral stationary phase with excellent resolution of various chiral compounds.[2,3,4,5] Okamoto and Yashima[5] reviewed the mechanism for discrimination between enantiomers of chiral compounds on polysaccharide phases studied by chromatographic, computational and spectroscopic methods. These studies indicated that the polysaccharide phases possess multiple interaction (say, hydrogen bonding and dipole-dipole interaction) sites with specific surface and cavities which are responsible for the chiral discrimination for a wide range of chiral compounds. The ability to recognize chirality must be affected by the local conformation of the polysaccharide chains, because the steric fit of enantiomers to the polysaccharide phases depends on the local conformation.

Recently, we have further investigated the helical conformation of amylose carbamates in various solvents through their dimensional and hydrodynamic properties in dilute solutions.[6,7,8] The chain stiffness and local helical structure estimated from the dilute solution properties were closely related to the ability of hydrogen-bonding between the solvent and carbamate groups of the polymer as well as bulkiness of the solvent and also of the substituent. Thus, we have concluded that the conformation of amylose carbamate chains is sensitively affected by the interaction with solvent molecules.

If the interaction of a chiral solvent with an amylose carbamate is substantially different from that of its enantiomer, the polymer conformation could be different in the enantiomer solvents, which may be detectable by dimensional and hydrodynamic properties. However, such solution properties of chiral polymers in chiral solvents have not been published to our knowledge whereas the difference in affinity of chiral agents is well reported in the past literature.[2,3,4,5,9]

In this study, we chose $_{D}$- and $_{L}$-lactates, which are commercially available and good solvents for some polysaccharide carbamates. Fig. 1 illustrates intrinsic viscosities [η] for some polysaccharide derivatives in chiral solvents, that is, amylose tris(*n*-butylcarbamate) (ATBC),[6] cellulose tris(phenylcarbamate),[10] and curdlan tris(phenylcarbamate)[11] in $_{D}$-, $_{DL}$- and $_{L}$-ethyl lactates (ELs), and

ATBC in methyl and *n*-butyl lactates; it should be noted that the weight-average molecular weights M_w of these samples range between 7×10^5 and 1.1×10^6. Intrinsic viscosity in the lactates appreciably increases or decreases with increasing D-lactates content ϕ_D. The $[\eta]$ data for ATBC in ELs have the most significant ϕ_D dependence in the five systems and that in D-ethyl lactate (D-EL) is indeed 42 % larger than that in L-ethyl lactate (L-EL), suggesting that this system is suitable for investigating chiral solvent effects on the dimensional and hydrodynamic properties of polysaccharides. We thus made light and smal$_L$-angle X-ray scattering and viscosity measurements on ATBC in the three ELs and analyzed the obtained data in terms of the wormlike chain[12] with excluded volume to determine the Kuhn segment length λ^{-1} (or, more generally, the chain stiffness parameter in the helical wormlike chain[13,14]) and the helix pitch (or contour length) per residue h, which is related to the local helical structure. In addition to these measurements, we investigated the difference of interactions of ATBC with D- and L-EL by isothermal calorimetric measurements.

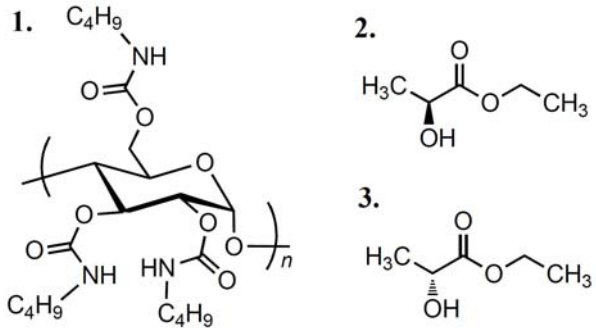

Chart 1 Chemical structures of **1**: amylose tris(*n*-butylcarbamate) (ATBC), **2**: L-ethyl lactate (L-EL), **3**: D-ethyl lactate (D-EL).

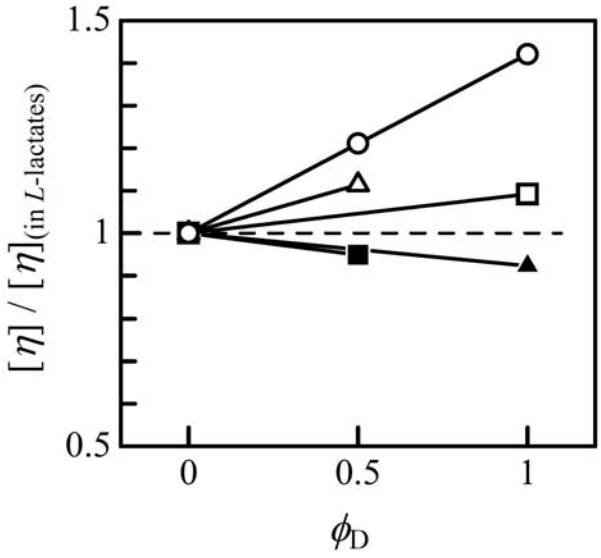

Fig. 1 Ratio of the intrinsic viscosity [η] to that in the $_{L}$-enantiomer plotted against the volume fraction ϕ_D of $_{D}$-enantiomer content at 25 °C. Open symbols: data points for ATBC900K in ELs (circles), *n*-butyl lactates (triangles) and ATBC700K in methyl lactates (squares). Filled symbols: data points for cellulose tris(phenylcarbamate) (triangles, M_w = 9.0 × 10^5) and curdlan tris(phenylcarbamate) (squares, M_w = 1.1 × 10^6) in ELs.

Experimental section

Samples and solvents

Previously investigated ten ATBC samples (ATBC1700K, ATBC900K, ATBC700K, ATBC490K, ATBC260K, ATBC130K, ATBC110K, ATBC55K, ATBC53K and ATBC17K) were chosen for this study and have no branching since they were made from enzymatically synthesized amylose, which has no branching and quite narrow molecular-weight distribution.[15] Their M_w ranges between 1.7 × 10^4 and 1.7 × 10^6 and the polydispersity indices were about 1.1.[6] $_{L}$-EL and $_{DL}$-ethyl lactate ($_{DL}$-EL) were purchased and purified by fractional distillation under reduced pressure. $_{D}$-EL was synthesized by interesterification from $_{D}$-methyl lactate (Musashino Chem. Lab. Ltd.) and ethanol with titanium tetraisopropoxide as a catalyst. The product was purified three times by fractional distillation and the purity of the resultant solvent were confirmed by ^{1}H-NMR. The specific optical rotation $[\alpha]_{500}$ at 500 nm wavelength was obtained to be 14.1 and –14.4 deg cm^{-2} g^{-1} for $_{D}$-EL and $_{L}$-EL, respectively.

Light and smal$_{L}$-angle X-ray scattering (SAXS)

SAXS measurements were made for ATBC55K and ATBC17K in $_{D}$-EL, $_{DL}$-EL and $_{L}$-EL at 25 °C with an imaging plate detector at the BL40B2 Beamline in SPring-8. The wavelength λ_0 in vacuum and the camera length were set to be 0.1 nm and 1500 mm, respectively. The experimental details including light scattering were reported previously.[6] ATBC17K in $_{L}$-EL was not studied because it did not completely dissolve in the solvent. The excess scattering intensities evaluated for four different polymer mass concentrations c were analyzed using the Berry square-root plot[16] to determine the particle scattering function $P(q)$ and the z-average mean square radius of gyration $\langle S^2 \rangle_z$.

Static light scattering (SLS) measurements were made for ATBC900K, ATBC490K and ATBC260K in the three ELs at 25 °C on a Fica-50 light scattering photometer with vertically polarized incident light at λ_0 = 436 nm. The obtained data for five different c was analyzed by means of the Berry square-root plot, to determine their $\langle S^2 \rangle_z$, M_w and the second virial coefficient. The specific refractive index increments $\partial n/\partial c$ for ATBC460K in the three ELs at 25 °C at λ_0 = 436 nm were determined to be 0.0725, 0.0718, 0.0707 cm^{3}g^{-1} in $_{D}$-EL, $_{DL}$-EL and $_{L}$-EL, respectively. The Berry square-root plot was used to determine their $\langle S^2 \rangle_z$, M_w and the second virial coefficient.

Viscometry

Solvent and solution viscosities for ATBC900K, ATBC700K, ATBC490K, ATBC260K, ATBC130K, ATBC110K and ATBC55K in the three ELs, ATBC1700K in $_{DL}$- and $_{L}$-EL, and ATBC17K in $_{DL}$-EL all at 25 °C were measured using an Ubbelohde type viscometer. The relative viscosity was determined by taking into account the difference between the solution and solvent densities.

Isothermal titration calorimetry (ITC)

Heats of dilution of $_{D}$- and $_{L}$-EL solutions of ATBC with the enantiomer ELs were estimated by using a VP-ITC calorimeter (Microcal). A $_{D}$-EL solution of ATBC ($c \sim 4.0 \times 10^{-2}$ g cm^{-3} for ATBC53K and 3.2×10^{-2} g cm^{-3} for ATBC460K) was dripped little by little (2 μL each at every 240 sec) into 2 mL of $_{L}$-EL to determine the amount of heat $q_{D,soln \rightarrow L,dil}$ at each dripping. Subscripts D, L, soln and dil indicate $_{D}$-EL, $_{L}$-EL, solution and diluent, respectively. These measurements were made by exchanging the solvent and/or diluent by the enantiomers to obtain $q_{L,soln \rightarrow D,dil}$, $q_{D,soln \rightarrow D,dil}$ and $q_{L,soln \rightarrow L,dil}$; $q_{D,soln \rightarrow D,dil}$ and $q_{L,soln \rightarrow L,dil}$ were negligibly smaller than $q_{L,soln \rightarrow D,dil}$ and $q_{D,soln \rightarrow L,dil}$. The same measurements were also made for the cellulose tris(phenylcarbamate) sample used for the preliminary viscosity measurement (see Fig. 1).

Results and discussion

Results from SLS, SAXS and viscometry

Angular dependence of $P(q)^{-1/2}$ for the ATBC samples in the three ELs is shown in Fig. 2. Each curve is convex upward, typical for semiflexible chains in solution. The $\langle S^2 \rangle_z$ values determined from the initial slope increase with increasing $_{D}$-EL content as is the case with $[\eta]$ in Fig. 1. Numerical results from SLS and SAXS were summarized in Table 1. The obtained M_w's for ATBC900K, ATBC460K and ATBC260K are almost equivalent to those reported in our previous paper,[6,7] indicating that ATBC samples are molecularly dispersed in the three ELs. The second virial coefficients are in a narrow range between $0.7 - 1.4 \times 10^{-4}$ mol g^{-2}cm^3. The three ELs are therefore good solvents for ATBC. Fig. 3 displays the resultant $\langle S^2 \rangle_z$ for the ATBC samples in the three ELs at 25 °C along with those in tetrahydrofuran (THF) and methanol (MeOH), in which ATBC behaves as rigid and loose (more flexible) helices, respectively.[6] The solvent dependence in the three ELs becomes more significant with increasing M_w but their $\langle S^2 \rangle_z$'s range between those in THF and MeOH, suggesting that ATBC in ELs has intermediate conformation between those in THF and MeOH. Similar behavior is also seen in the $[\eta]$ data, for which the molecular weight dependencies in the five solvents are illustrated in Fig. 4. The data for ATBC in $_{D}$-EL are systematically larger than that for the same sample in $_{L}$-EL.

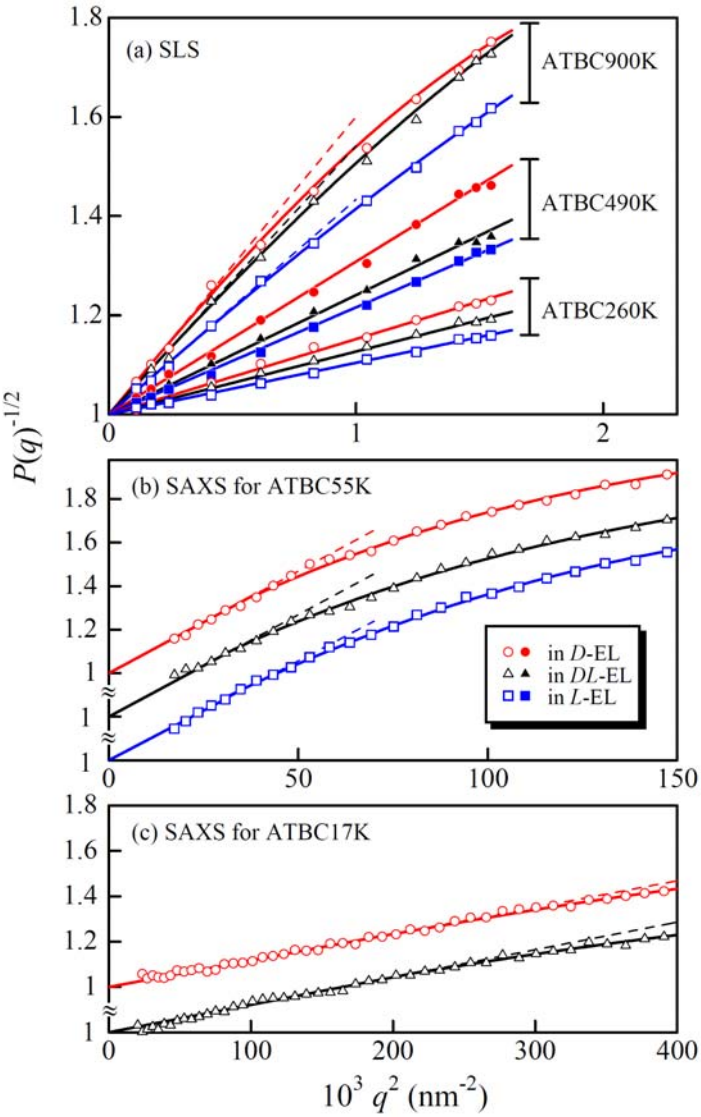

Fig. 2 Berry Plots for indicated ATBC samples in $_{D}$-EL (circles), $_{DL}$-EL (triangles) and $_{L}$-EL (squares) at 25 °C: (a) SLS for ATBC900K, ATBC490K and ATBC260K, (b) SAXS for ATBC55K, and (c) SAXS for ATBC17K.

Table 1 Results from SLS and SAXS measurements on ATBC samples in $_{D}$-EL, $_{DL}$-EL and $_{L}$-EL at 25 °C

sample	in $_{D}$-EL		in $_{DL}$-EL		in $_{L}$-EL	
	$M_w/10^4$	$\langle S^2\rangle_z^{1/2}$ (nm)	$M_w/10^4$	$\langle S^2\rangle_z^{1/2}$ (nm)	$M_w/10^4$	$\langle S^2\rangle_z^{1/2}$ (nm)
ATBC900K [a]	87.0	60	87.0	57	89.5	51
ATBC490K [a]	50.5	43.0	49.5	38.0	51.0	36.0
ATBC260K [a]	24.3	30.2	24.8	27.6	25.4	25.0
ATBC55K	5.45 [c]	7.5 [b]		7.5 [b]		7.4 [b]
ATBC17K	1.66 [c]	2.65 [b]		2.70 [b]		

[a] SLS. [b] SAXS. [c] From sedimentation equilibrium in methanol (ref. 6).

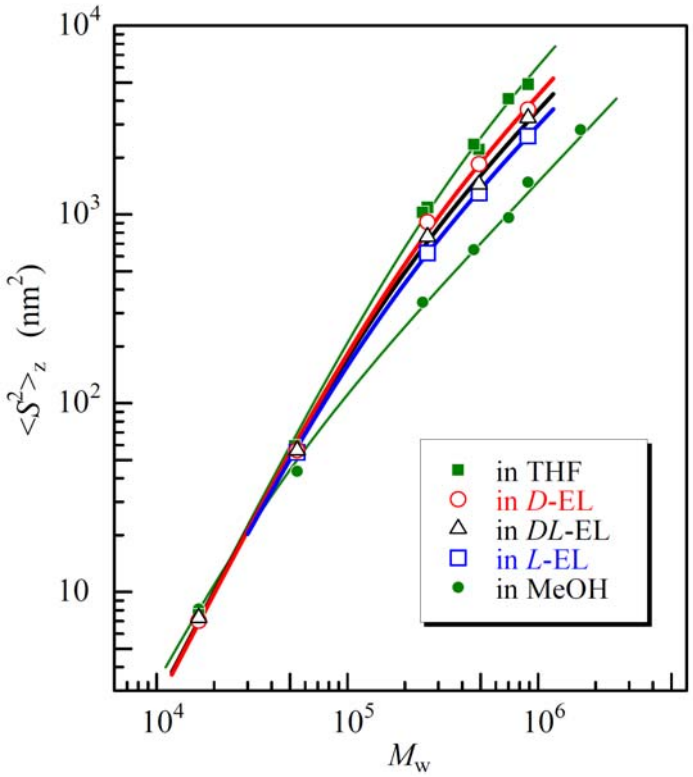

Fig. 3 Molecular weight dependence of $\langle S^2 \rangle_z$ for ATBC in $_D$-EL (open circles), $_{DL}$-EL (triangles), $_L$-EL (open squares), THF[6] (filled squares) and MeOH [6] (filled circles) at 25 °C. Curves: theoretical values calculated for the wormlike chain with the parameters in Table 2.

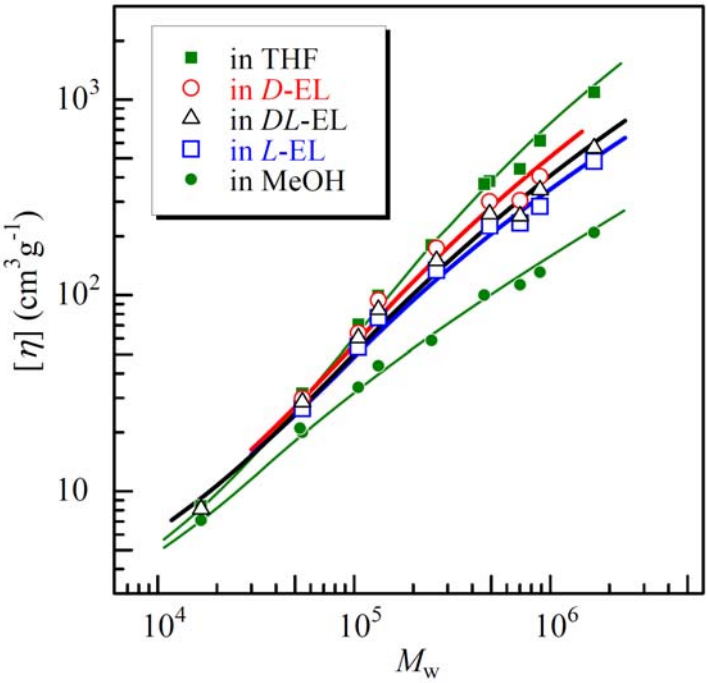

Fig. 4 Molecular weight dependence of $[\eta]$ for ATBC in $_D$-EL (open circles), $_{DL}$-EL (triangles), $_L$-EL (open squares), THF[6] (filled squares) and MeOH[6] (filled circles) at 25 °C. Curves: theoretical values calculated for the wormlike cylinder with the parameters in Table 2.

Wormlike Chain Analysis

Radius of Gyration. The molecular weight dependence of $\langle S^2\rangle_z$ for ATBC in the three ELs was analyzed in terms of the unperturbed wormlike chain,[12] for which the mean-square radius of gyration $\langle S^2\rangle$ is expressed as[17]

$$\left\langle S^2 \right\rangle = \frac{M}{6\lambda M_L} - \frac{1}{4\lambda^2} + \frac{M_L}{4\lambda^3 M} - \frac{M_L^2}{8\lambda^4 M^2}\left[1 - \exp\left(-\frac{2\lambda M}{M_L}\right)\right] \qquad (1)$$

The molar mass per unit contour length M_L and λ^{-1} were unequivocally determined from the curve fitting procedure and the obtained parameters are summarized in Table 2. Theoretical values calculated with the parameters are drawn in Fig. 3 as solid curves, which fit the experimental $\langle S^2\rangle_z$ almost quantitatively. It should be noted that the exclude$_D$-volume effects were found to be negligible when the effect is taken into account by the quasi-two-parameter (QTP) theory[13,18] and the

Domb-Barrett function.[19] This is reasonable because the Kuhn segment number (=λL) is at most 15 even for the highest M_w sample, and furthermore the effect is mostly negligible for ATBC in MeOH in which the ATBC chain is more flexible (see Table 3) and the second virial coefficients are comparable to those for ATBC in ELs.

Table 2 Wormlike-chain parameters for ATBC in $_D$-EL, $_{DL}$-EL and $_L$-EL at 25 °C

method	M_L (nm^{-1})	λ^{-1} (nm)	d (nm)
in $_D$-EL			
$\langle S^2\rangle_z$	1770 ± 50	52 ± 4	
$P(q)$	1830 ± 30	49 [a]	
$[\eta]$	1800 [a]	45 ± 5	3.5 ± 0.3
in $_{DL}$-EL			
$\langle S^2\rangle_z$	1730 ± 50	41 ± 3	
$P(q)$	1830 ± 40	38 [a]	
$[\eta]$	1780 [a]	35 ± 3	3.3 ± 0.2
in $_L$-EL			
$\langle S^2\rangle_z$	1750 ± 100	34 ± 2	
$P(q)$	1770 ± 30	32 [a]	
$[\eta]$	1760 [a]	29 ± 2	3.4 ± 0.3

[a] Assumed values.

For cylindrical wormlike chain with the chain diameter d, the radius of gyration is estimated to be $\langle S^2\rangle + d^2/8$.[20] This parameter may be approximately estimated from the cross-sectional plot[21] [ln $qP(q)$ vs q^2] as illustrated for ATBC in the ELs in Fig. 5, along with those in THF and MeOH.[6] It should be noted that this approximation is fairly good for wormlike cylinders.[22] While the estimated d value (see Fig. 5) in THF and MeOH is consistent with those determined from the analysis in terms of the wormlike chain as reported previously,[6] the plots in ELs have positive slopes, and hence negative d^2. This is most likely due to the electron density profile around the chain contour including solvent molecules and/or the local helical structure of the polymer. Indeed, such negative d^2 values are reported for some other systems,[23,24] and furthermore, some core shell cylinder[25] with appropriate electron densities can reproduce the negative d^2 (see ESI). In any case, the obtained $d^2/8$ (~ −0.05 nm^2) is negligibly smaller than the $\langle S^2\rangle_z$ for the smallest M_w sample in ELs.

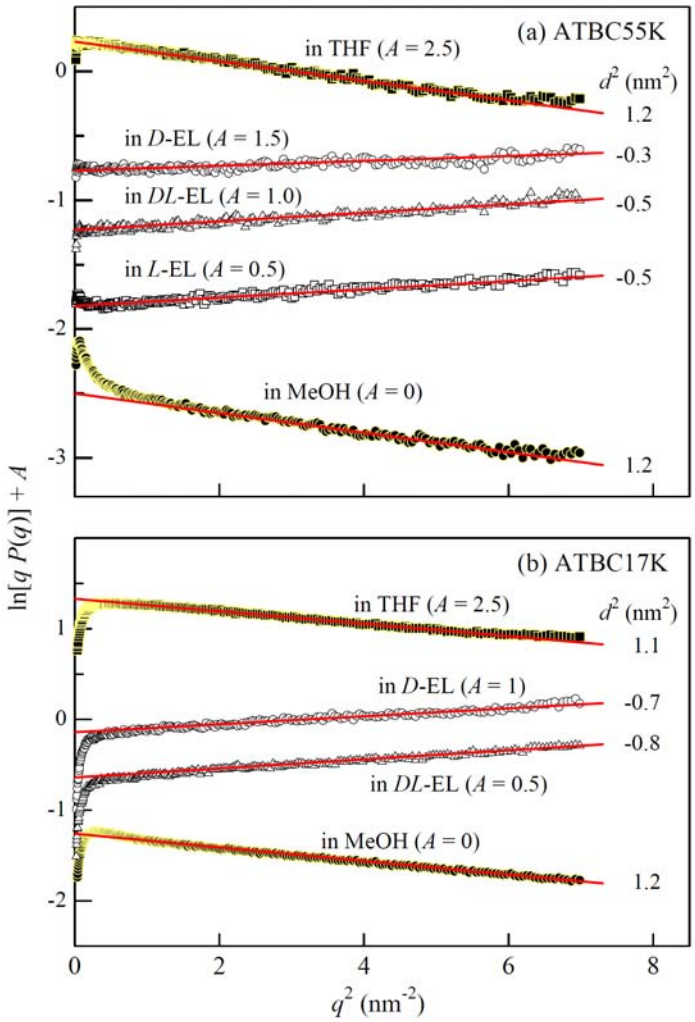

Fig. 5 Cross-sectional plots for (a) ATBC53K (in THF) or ATBC55K (in other solvents) and (b) ATBC17K in $_{D}$-EL (open circles), $_{DL}$-EL (triangles), $_{L}$-EL (open squares), THF[6] (filled squares) and MeOH[6] (filled circles) at 25 °C.

Particle Scattering Function. The scattering function for the corresponding thin chain may be experimentally estimated as $P(q)\exp(q^2d^2/16)$. The Holtzer plots, [26] that is, $qP(q)$ and $qP(q)\exp(q^2d^2/16)$ plotted against q, are illustrated in Fig. 6. The difference between $qP(q)\exp(q^2d^2/16)$ and $qP(q)$ is quite small for small q. Since the wide Holtzer plateau is seen in $qP(q)$ $\exp(q^2d^2/16)$ at $q > 0.5$ nm^{-1} for ATBC55K and at $q > 0.7$ nm^{-1} for ATBC17K, the contour length and hence M_L may be determined from the height of the plateau. The theoretical $qP(q)$'s for thin rod (dashed lines, mostly hidden behind the solid curves) with the estimated contour length reproduce the experimental Holtzer plateau almost quantitatively but are slightly smaller than the experimental data at the low q region ($q < 0.5$ nm^{-1}) owing to the effect of the chain flexibility.

Indeed, the calculated $qP(q)$ by using the Nakamura-Norisuye equation[27] for thin wormlike chains with the mean λ^{-1} value (see Table 2) determined from $\langle S^2 \rangle_z$ and $[\eta]$ excellently trace the experimental data.

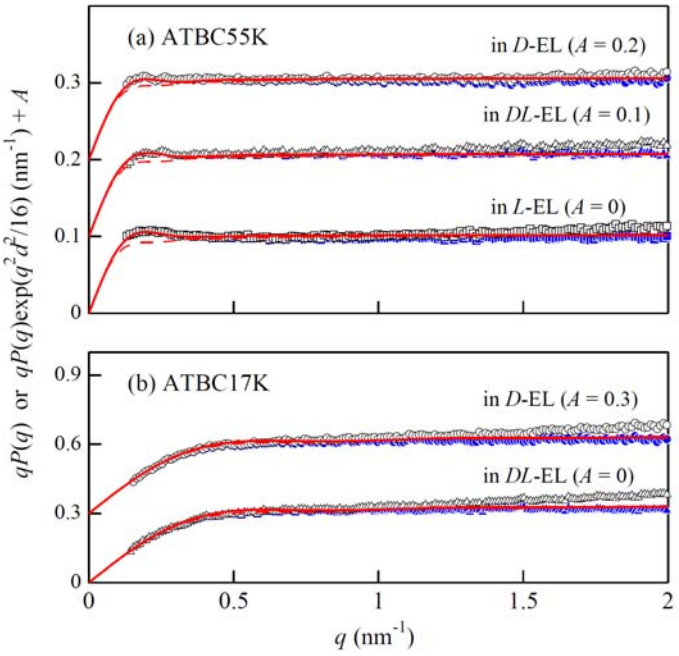

Fig. 6 Holtzer Plots for ATBC samples in $_{D}$-EL (circles), $_{DL}$-EL (triangles) and $_{L}$-EL (squares) at 25 °C. Open symbols: $qP(q)$. Filled symbols: $qP(q)\exp(q^2d^2/16)$ with the d^2 value presented in Fig. 5.

Intrinsic Viscosity. The Yamakawa-Fujii-Yoshizaki theory[13,28] for the unperturbed wormlike cylinder was used to analyze the molecular weight dependence of $[\eta]$ in ELs since the exclude$_{D}$-volume effects for $\langle S^2 \rangle$ are negligible. Thus, theoretical $[\eta]$ may be calculated from the three parameters, that is, M_L, λ^{-1} and d. When we assume the mean M_L value from $P(q)$ and $\langle S^2 \rangle_z$, λ^{-1} and d are unequivocally determined from the curve fitting and the resultant parameters are listed in Table 2; they are consistent with those from $P(q)$ and $\langle S^2 \rangle_z$, and consequently, we may conclude that accurate wormlike-chain parameters were determined for ATBC in the three ELs at 25 °C.

Relation between λ^{-1} and h

The mean λ^{-1} and h values for ATBC in the three ELs were summarized in Table 3 along with those in THF and MeOH.[6] The latter parameter was calculated from M_L by $h = M_0/M_L$ with M_0 being the molar mass of the ATBC repeat unit. While λ^{-1} in $_D$-EL is 53% larger than that in $_L$-EL, both h and λ^{-1} in ELs are in between those in THF and MeOH. In our previous study for ATBC in nine solvents,[7] we found that both h and λ^{-1} are functions of the number fraction of intramolecular hydrogen bonds f_{hyd} (f_{1698} in refs 6 and 7) determined from the amide I band (mainly C=O stretching) in the infrared absorption (IR) spectra, and their functions are consistent with the two states wormlike chain (TSWC) model[29] (cf. ESI) in which each contour point along the chain takes the semiflexible (loosely helical) and rodlike (rigid helical) sequences independently. This indicates that the conformational change of ATBC in various solvents may not be cooperative in contrast with, e.g., the helix-coil transition of polypeptides.

Since f_{hyd} cannot be determined directly from IR in ELs because of the absorption of the solvents, we estimate f_{hyd} from the relation between λ^{-1} and h using the following equation for the TSWC model.

$$h^{-1} - h_F^{-1} = -\frac{h_R^{-1} - h_F^{-1}}{\lambda_F - \lambda_R}(\lambda - \lambda_F) \qquad (2)$$

Here, h_R and h_f denote h for rigid and semiflexible part chains, respectively, and λ_R^{-1} and λ_f^{-1} are the Kuhn segment length for the corresponding part chains, respectively. This equation is derived from the combination of eqs (S2) in the ESI. Fig. 7 shows the plots of h^{-1} vs λ in the three ELs along with the nine previously determined values.[7] The current three data points were well fitted by our previous data, indicating that the independent two-state model is also applicable for ATBC in ELs. This allows us to estimate f_{hyd} by using the relationship

$$\lambda h = 0.029\left(1 - \frac{f_{hyd}}{0.55}\right) \qquad (3)$$

obtained from the solid line in Fig. 9d in ref. 7. The estimated f_{hyd} are listed in Table 3 and the f_{hyd} in $_{D}$-EL is 15 % larger than that in $_{L}$-EL. This indicates that the number of intramolecular H-bonding of ATBC depends on the chirality of the solvent.

Table 3 Values of the helix pitch per residue h, the Kuhn segment length λ^{-1} and the number fraction of intramolecularly H-bonding C=O groups for ATBC at 25 °C

Solvent	h (nm)	λ^{-1} (nm)	f_{hyd}
THF [a]	0.26 ± 0.01	75 ± 5	0.52 [b]
$_{D}$-EL	0.255 ± 0.01	49 ± 4	0.47 [c]
$_{DL}$-EL	0.258 ± 0.01	38 ± 3	0.43 [c]
$_{L}$-EL	0.261 ± 0.01	32 ± 2	0.41 [c]
MeOH [a]	0.32 ± 0.01	11 ± 2	0 [b]

[a] Ref. 6. [b] From IR spectra in ref 6. [c] From eq 3

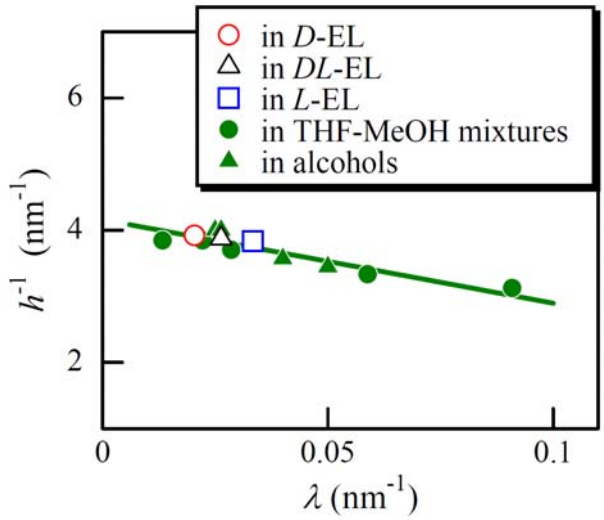

Fig. 7 Plots of h^{-1} vs λ for ATBC in $_{D}$-EL (an open circle), $_{DL}$-EL (an open triangle) and $_{L}$-EL (a square), THF-MeOH mixtures (filled circles),[6] and various alcohols (filled triangles).[7]

Thermal Analysis of ATBC in Ethyl Lactates.

If the number of intramolecular H-bonds of ATBC is different in the enantiomeric ELs, it should be detectable by isothermal titration calorimetry (ITC). Fig. 8 shows the time course of heat flow of the ITC measurements. An appreciable endothermic sharp peak appears when we added 2 μL each of EL solutions of ATBC into 2 mL of the enantiomer diluent. In the case that a $_{D}$-EL solution of

ATBC is added into pure L-EL, peaks were significantly higher than the opposite case, that is, L-solution was dripped into D-diluent.

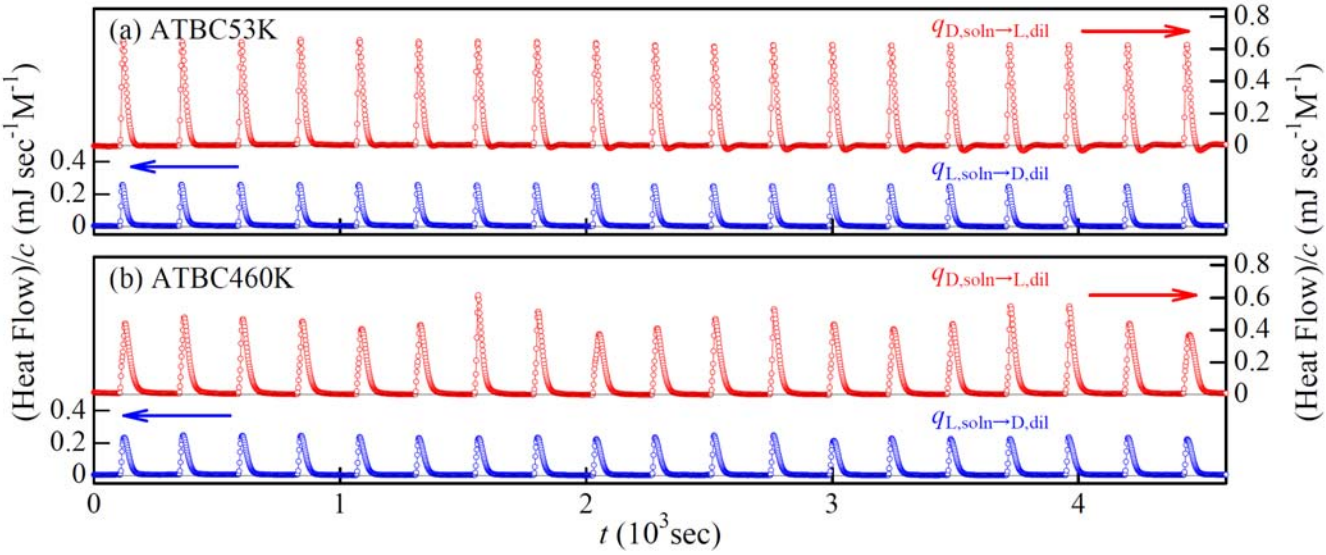

Fig. 8 Isothermal titration calorimetric data for ATBC53K (a) and ATBC460K (b) in ELs at 25 °C. 2 μL solution was dropped at every 2 min.

As explained in ESI, experimentally obtained heats of dilution $q_{D,soln\rightarrow L,dil}$, $q_{L,soln\rightarrow D,dil}$, $q_{D,soln\rightarrow D,dil}$ and $q_{L,soln\rightarrow L,dil}$ are written in terms of the intermolecular (or inter-segmental) attractive potential energies ε_{ij} between species i and j, on the basis of the lattice model.[30] When the volume of diluent is enough larger than that of solution, we obtain the following relation of the difference among the heats at dilution

$$\left(q_{D,soln\rightarrow L,dil}-q_{D,soln\rightarrow D,dil}\right)-\left(q_{L,soln\rightarrow D,dil}-q_{L,soln\rightarrow L,dil}\right)=2n_p z\left(\varepsilon'_{LP}-\varepsilon'_{DP}\right) \quad (4)$$

where z is the coordination number, n_p is the number of repeat units of ATBC in the diluted solution, and ε'_{LP} (ε'_{DP}) is the attractive potential energies between L-EL (D-EL) and the repeat unit of ATBC. The suitable choice of the repeating unit of ATBC is also mentioned in ESI. Since n_p is equal to $v_s c/M_0 N_A$ where N_A is the Avogadro number, c is the polymer mass concentration in the original

solution before dilution, and v_s is the volume of each drop (2 μL), the molar excess interaction energy $N_A z(\varepsilon'_{LP} - \varepsilon'_{DP})$ is related to be the experimental heat of dilution values as

$$N_A z\left(\varepsilon'_{LP} - \varepsilon'_{DP}\right) = \frac{\left(q_{D,soln\rightarrow L,dil} - q_{D,soln\rightarrow D,dil}\right) - \left(q_{L,soln\rightarrow D,dil} - q_{L,soln\rightarrow L,dil}\right)}{2v_s c/M_0} \qquad (5)$$

Substituting the mean heats of dilution values obtained for the second to 25th drops, $N_A z(\varepsilon'_{LP} - \varepsilon'_{DP})$ are estimated to be 2.4 kJ mol^{-1} and 2.3 kJ mol^{-1} for ATBC460K and ATBC53K, respectively. The positive value of $N_A z(\varepsilon'_{LP} - \varepsilon'_{DP})$ indicates that the interaction between ATBC and $_D$-EL stabilizes the polymer more than that between ATBC and $_L$-EL.

There are the following two interpretations for the result of $N_A z(\varepsilon'_{LP} - \varepsilon'_{DP})$.

(1) The number of hydrogen bonds between ATBC and $_D$-EL is larger than that between ATBC and $_L$-EL.

(2) While the number of the polymer-solvent hydrogen bonds is unaltered in $_D$-EL and $_L$-EL, the number of intramolecular hydrogen bonds of ATBC in $_D$-EL is larger than that in $_L$-EL. It is noted that the dissociation energy of the intramolecular hydrogen bonding by the interaction with the solvent is included in ε'_{LP} and ε'_{DP}.

As mentioned in the preceding subsection, the results of h and λ^{-1} are consistent with the interpretation (2). Both ELs may form the hydrogen bonding with the amide group of ATBC, but this hydrogen bonding may affect the internal rotation of the glucosidic linkage of ATBC or h probably due to the steric hindrance between the solvent and polymer. The interpretation (2) implies that the hydrogen bonding between ATBC and $_L$-EL enlarges h more to prohibit the intramolecular hydrogen bonding.

Interestingly, the obtained $N_A z(\varepsilon'_{LP} - \varepsilon'_{DP})$ for ATBC is significantly larger than that for cellulose tris(phenylcarbamate) (CTPC) (< 0.3 kJ mol^{-1}) for which the $[\eta]$ is almost irrespective of enantiomer excess of ELs (see Fig. 1). The polymer-solvent hydrogen bonding in both $_L$-EL and $_D$-EL may not affect or equally affect the internal rotation about the glucosidic linkage of CTPC.

If the large $N_A z(\varepsilon'_{LP} - \varepsilon'_{DP})$ for ATBC is mainly due to the difference in the number of intramolecular hydrogen bonds of ATBC in $_D$-EL and $_L$-EL, it may be related to the reduction of the intramolecular hydrogen bonding by

$$N_A z\left(\varepsilon'_{LP} - \varepsilon'_{DP}\right) \approx 3\left(f_{hyd,D} - f_{hyd,L}\right) N_A \varepsilon_H \quad (6)$$

since the repeat unit of ATBC has three C=O and NH groups. Here, $f_{hyd,D}$ and $f_{hyd,L}$ are f_{hyd} for ATBC in $_D$-EL and $_L$-EL, respectively, and ε_H is the hydrogen bonding energy. Using $f_{hyd,D}$ and $f_{hyd,L}$ in Table 3, we may estimate $N_A\varepsilon_H$ to be –13 kJ mol^{-1}, which is adequate as the hydrogen bonding energy.[31] This result supports our conclusion that the difference of the chain conformation of ATBC in $_D$-EL and $_L$-EL reflects the difference in the intramolecular hydrogen bonding of ATBC in the two solvents.

Conclusions

Both dimensions and intrinsic viscosities of ATBC in $_D$-EL are appreciably larger than that in $_L$-EL. This is mainly due to the 53% higher Kuhn segment length in $_D$-EL. The relationship between the Kuhn segment length and the helix pitch per residue for ATBC in $_D$-EL, $_{DL}$-EL and $_L$-EL is explained in terms of the independent two-state model consisting of random sequences of rodlike and semiflexible portions as is the case with ATBC in previously investigated nine solvents; hence, the number fraction of H-bonding C=O groups f_{hyd} is estimated. The 6% difference in f_{hyd} compared favorably with the difference in the heat of dilution of EL solutions of ATBC by $_L$- and $_D$-EL.

Acknowledgements

The authors thank Prof. Akira Harada, Prof. Hiroyasu Yamaguchi and Dr. Motofumi Osaki (Osaka Univ.) for isothermal titration calorimetry measurements. The synchrotron radiation experiments were performed at the BL40B2 in SPring-8 with the approval of the Japan Synchrotron Radiation Research Institute (JASRI) (Proposal #2007A1034, #2007B1296 and #2008A1313). This work was

partially supported by Grant-in-Aid for Young Scientists (#23750128) from Japan Society for the Promotion of Science (JSPS).

References

1 W. Burchard, in *Soft-Matter Characterization*, eds. R. Borsali and R. Pecora, Springer, Berlin, Germany, 2008, pp. 465-603.

2 T. Ikai and Y. Okamoto, *Chem. Rev*., 2009, **109**, 6077-6101.

3 Y. Okamoto, *J. Polym. Sci. Part A: Polym. Chem*., 2009, **47**, 1731-1739.

4 C. Yamamoto and Y. Okamoto, *Bull. Chem. Soc. Jpn*., 2004, **77**, 227-257.

5 Y. Okamoto and E. Yashima, *Angew. Chem. Int. Ed*., 1998, **37**, 1020-1043.

6 K. Terao, M. Murashima, Y. Sano, S. Arakawa, S. Kitamura and T. Norisuye, *Macromolecules*, 2010, **43**, 1061-1068.

7 Y. Sano, K. Terao, S. Arakawa, M. Ohtoh, S. Kitamura and T. Norisuye, *Polymer* 2010, **51**, 4243-4248.

8 K. Terao, T. Fujii, M. Tsuda, S. Kitamura and T. Norisuye, *Polym. J*., 2009, **41**, 201-207; T. Fujii, K. Terao, M. Tsuda, S. Kitamura and T. Norisuye, *Biopolymers*, 2009, **91**, 729-736; M. Tsuda, K. Terao, Y. Nakamura, Y. Kita, S. Kitamura and T. Sato, *Macromolecules*, 2010, **43**, 5779-5784.

9 C. Yamamoto, E. Yashima and Y. Okamoto, *J. Am. Chem. Soc*., 2002, **124**, 12583-12589; R. B. Kasat, Y. Zvinevich, H. W. Hillhouse, K. T. Thomson, N.-H. L. Wang, E. I. Franses, *J. Phys. Chem. B*., 2006, **110**, 14114-14122; R. M. Wenslow Jr. and T. Wang, *Anal. Chem*., 2001, **73**, 4190-4195; R. M. Wenslow Jr. and T. Wang, *J. Chromatogr. A*., 2003, **1015**, 99-110; S. Ma, S. Shen, H. Lee, N. Yee, C. Senanayake, L. A. Nafie and N. Grinberg, *Tetrahedron: Asymmetry*, 2008, **19**, 2111-2114; R. B. Kasat , E. I. Franses and N. H. L. Wang, *Chirality*, 2010, **22**, 565-579; Y. Li, D. Liu, P. Wang and Z. Zhou, *J. Sep. Sci.*, 2010, **33**, 3245-3255; C. West, G. Guenegou, Y. Zhang and L. Morin-Allory, *J. Chromatogr. A.*, 2011, **1218**, 2033-2057.

10 F. Kasabo, T. Kanematsu, T. Nakagawa, T. Sato and A. Teramoto, *Macromolecules*, 2000, **33**, 2748-2756.

11 T. Ochiai, Y. Nakamura, C. Yoshikawa, K. Terao and T. Sato, in preparation.

12 O. Kratky and G. Porod, *Recl. Trav. Chim. Pays-Bas*, 1949, **68**, 1106-1122.

13 H. Yamakawa, *Helical Wormlike Chains in Polymer Solutions*, Springer, Berlin, Germany, 1997.

14 H. Yamakawa, *Polym. J.*, 1999, **31**, 109-119.

15 S. Kitamura, H. Yunokawa, S. Mitsuie and T. Kuge, *Polym. J.*, 1982, **14**, 93-99; H. Waldmann, D. Gygax, M. D. Bednarski, W. R. Shangraw and G. M. Whitesides, *Carbohydr. Res.*, 1986, **157**, c4-c7.

16 G. C. Berry, *J. Chem. Phys.*, 1966, **44**, 4550-4564.

17 H. Benoit and P. Doty, *J. Phys. Chem.*, 1953, **57**, 958-963.

18 H. Yamakawa and W. H. Stockmayer, *J. Chem. Phys.*, 1972, **57**, 2843-2854; J. Shimada and H. Yamakawa, *J. Chem. Phys*., 1986, **85**, 591-599.

19 C. Domb and A. J. Barrett, *Polymer*, 1976, **17**, 179-184.

20 T. Konishi, T. Yoshizaki, T. Saito, Y. Einaga and H. Yamakawa, *Macromolecules*, 1990, **23**, 290-297.

21 O. Glatter and O. Kratky, *Small Angle X-Ray Scattering*, Academic Press, London, U. K., 1982.

22 Y. Nakamura and T. Norisuye, *J. Polym. Sci., Part B: Polym. Phys.*, 2004, **42**, 1398-1407.

23 P. Hickl, M. Ballauff, U. Scherf, K. Müllen and P. Lindner, *Macromolecules*, 1997, **30**, 273-279.

24 K. Terao, K. Mizuno, M. Murashima, Y. Kita, C. Hongo, K. Okuyama, T. Norisuye and H. P. Bächinger, *Macromolecules*, 2008, **41**, 7203-7210.

25 I. Livsey, *J. Chem. Soc. Faraday. Trans. 2,* 1987, **83**, 1445-1452.

26 A. J. Holtzer, *Polym. Sci*., 1955, **17**, 432-434.

27 Y. Nakamura and T. Norisuye, in *Soft-Matter Characterization*, eds. R. Borsali and R. Pecora, Springer, Berlin, Germany, 2008, p 236-286.

28 H. Yamakawa and M. Fujii, *Macromolecules*, 1974, **7**, 128-135; H. Yamakawa and T. Yoshizaki, *Macromolecules*, 1980, **13**, 633-643.

29 S. Chisaka and T. Norisuye, *J. Polym. Sci., Part B: Polym. Phys.*, 2001, **39**, 2071-2080.

30 P. J. Flory, *Principles of Polymer Chemistry*, Cornell University Press, Ithaca, NY, USA, 1953.

31 L. Pauling, *The Nature of the Chemical Bond*, Cornell University Press, Ithaca, NY, USA, 1960.

Graphical abstract

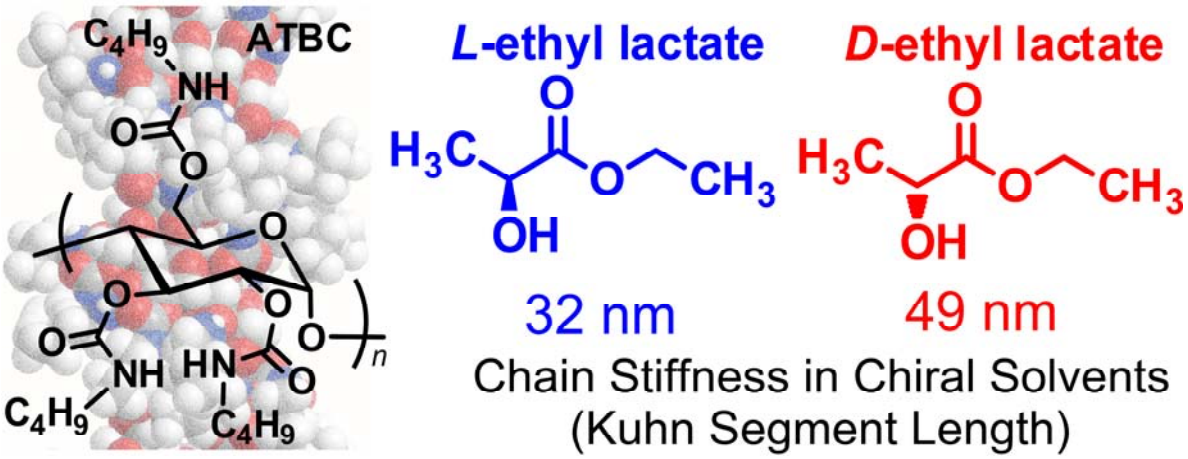

A chiral polysaccharide derivative, amylose tris(*n*-butylcarbamate), has 52% higher chain stiffness in $_{D}$-ethyl lactate than that in $_{L}$-ethyl lactate.

Electronic Supplementary Information

Conformational Change of a Amylose Derivative in Chiral Solvents: Amylose Tris(*n*-butylcarbamate) in Ethyl Lactates

Shota Arakawa, Ken Terao,* Shinichi Kitamura, and Takahiro Sato

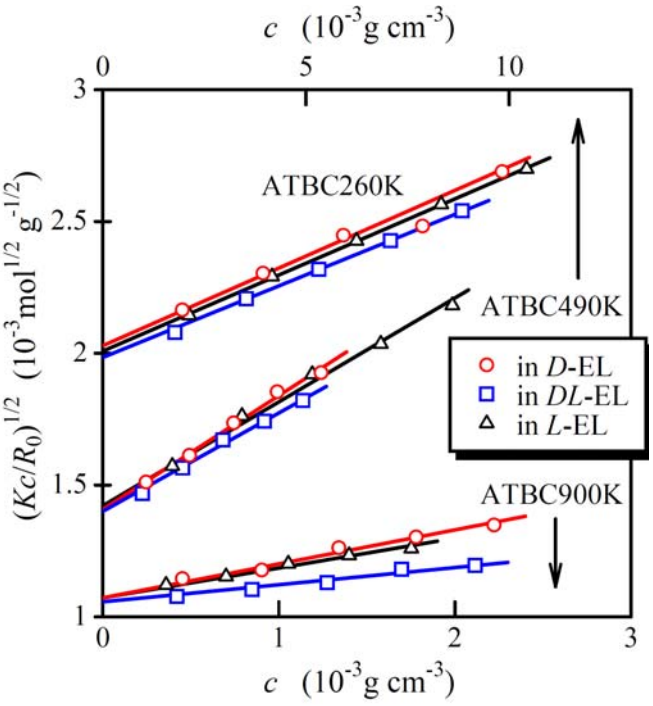

Fig. S1. Polymer mass concentration c dependence of $(Kc/R_0)^{1/2}$ for indicated ATBC samples in *D*-EL (red circles), *DL*-EL (black triangles), and *L*-EL (blue triangles) at 25 °C.

Cross Sectional Plot for a Core-Shell Cylinder Model. To demonstrate the negative d^2 for ATBC in ELs, we calculated $P(q)$ for a core-shell cylinder with the length L by[1]

$$P(q)=\int_0^{2\pi}\left|\frac{d_\mathrm{i}^2\Delta\rho_\mathrm{i}G(q,\theta,d_\mathrm{i})+d_\mathrm{o}^2\Delta\rho_\mathrm{o}G(q,\theta,d_\mathrm{o})-d_\mathrm{i}^2\Delta\rho_\mathrm{o}G(q,\theta,d_\mathrm{o})}{(\Delta\rho_\mathrm{i}-\Delta\rho_\mathrm{o})d_\mathrm{i}^2+\Delta\rho_\mathrm{o}d_\mathrm{o}^2}\right|\sin\theta\,\mathrm{d}\theta \qquad \text{(S1)}$$

with

$$G(q,\theta,d_\mathrm{x})=\frac{\sin\left[(qL/2)\cos\theta\right]J_1\left[(qd_\mathrm{x}/2)\sin\theta\right]}{\left[(qL/2)\cos\theta\right]\left[(qd_\mathrm{x}/2)\sin\theta\right]} \qquad \text{(S2)}$$

where d_i and d_o are the diameter of the inner (or core) and outer (or shell) cylinders, $\Delta\rho_i$ and $\Delta\rho_o$ the corresponding excess electron densities. The obtained ln[q $P(q)$] from eq S1 with L = 40 nm, d_i = 0.8 nm, d_o = 1.2 nm, $\Delta\rho_i$ = 1.1, and $\Delta\rho_o$ = 0.963 are plotted against q^2 (the cross-sectional plot) in Fig. S2. They have a positive slope and are well fitted by the straight line calculated by the following approximate equation[2]

$$P(q) = \left\{ \frac{\mathrm{Si}(qL)}{qL/2} - \left[\frac{\mathrm{Sin}(qL/2)}{qL/2} \right]^2 \right\} \exp\left(-\frac{q^2 d^2}{16} \right) \qquad \text{(S3)}$$

when we choose with L = 40 nm and d^2 = –0.5 nm^2. This indicates that a core-shell model may explain the negative d^2. It should be however noted that the obtained parameters might not be useful to know the detail electron density of ATBC since the scattering function at this q range is also affectable by the local helical structure and distribution of solvent molecules nereby the polymer chain.

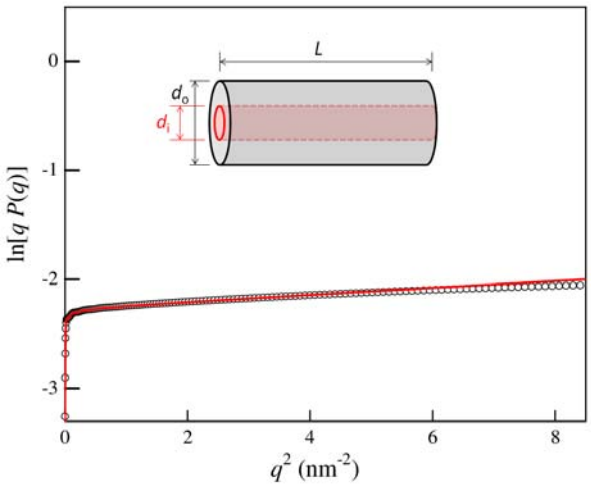

Fig. S2. Cross sectional plots for a core-shell cylinder model (circles) calculated from eq S1 with L = 40 nm, d_i = 0.8 nm, d_o = 1.2 nm, $\Delta\rho_i$ = 1.1, and $\Delta\rho_o$ = 0.963. Solid line, calculated from eq S3 with L = 40 nm and d^2 = –0.5 nm^2.

Two-States Wormlike Chain (TSWC) Model. The TSWC model is defined as the continuous limit of a freely rotating chain of N bonds in which each bond can take two states: the state 1 with the length b_1, bond angle θ_1, and probability f_1, and the state 2 with the length b_2, bond angle θ_2, and probability f_2. The continuous chain is obtained by taking the limit $N \to \infty$, $b_1 \to 0$, $b_2 \to 0$, $\theta_1 \to \pi$, and $\theta_2 \to \pi$ under the conditions that the following four parameters are constant:

$$Nb_1 = N_0 h_1, \quad Nb_2 = N_0 h_2, \quad \frac{1-\cos\theta_1}{2b_1} = \lambda_1, \quad \frac{1-\cos\theta_2}{2b_2} = \lambda_2 \tag{S4}$$

where N_0 is the degree of polymerization, h_1 and h_2 are the contour lengths per monomer unit in the states 1 and 2, respectively [$N_0 h_1$ ($N_0 h_2$) is the contour length of the chain at $f_1 = 1$ ($f_2 = 1$)], and λ_1^{-1} and λ_2^{-1} are the Kuhn segment lengths in the states 1 and 2, respectively. If appearances of states 1 and 2 are completely independent along the chain, we can show that expressions for dimensional and hydrodynamic properties of the TSWC model are identical with those for the original wormlike chain model with the contour length per monomer unit h and the Kuhn segment length λ calculated by[3,4]

$$h \equiv f_1 h_1 + f_2 h_2, \quad \lambda \equiv \left(f_1 h_1 \lambda_1 + f_2 h_1 \lambda_1 \right) / \left(f_1 h_1 + f_2 h_2 \right) \tag{S5}$$

Heat of Dilution and Polymer-Solvent Interaction Parameter. Let us consider the dilution process of a polymer solution with a diluent. The diluent, the solvent (in the polymer solution), and polymer are denoted as components 0, 1, and 2, respectively. Using the lattice model,[5] we may write enthalpies of the pure systems of compnents 0, 1, and 2 by

$$H_0 = \tfrac{1}{2} z n_0 \varepsilon_{00},\ \ H_1 = \tfrac{1}{2} z n_1 \varepsilon_{11},\ \ H_2 = \tfrac{1}{2} z n_2 \varepsilon_{22} \tag{S6}$$

where n_0, and n_1 are the numbers of diluent and solvent molecules, n_2 is the number of structural units of the polymer with the same volume as that of the diluent and solvent molecules, z is the coordination number, and ε_{ii} (i = 0, 1, and 2) are the intermolecular (or inter-segmental) attractive potential energies. It is noted that ε_{ii}'s are negative and their absolute values are larger for stronger interaction. According to van Laar and Scachard,[3] the heat of dilution of the polymer solution with the diluent is written as

$$\Delta H_{0+12} = \frac{z n_0 \left\{ {n_1}^2 \left[\varepsilon_{01} - \tfrac{1}{2}(\varepsilon_{00} + \varepsilon_{11}) \right] + n_1 n_2 \left(\varepsilon_{01} + \varepsilon_{02} - \varepsilon_{00} - \varepsilon_{12} \right) + {n_2}^2 \left[\varepsilon_{02} - \tfrac{1}{2}(\varepsilon_{00} + \varepsilon_{22}) \right] \right\}}{\left(n_0 + n_1 + n_2 \right)\left(n_1 + n_2 \right)} \tag{S7}$$

When the diluent and solvent are *L*-EL and *D*-EL, respectively, $\varepsilon_{00} = \varepsilon_{\mathrm{LL}} = \varepsilon_{\mathrm{DD}} = \varepsilon_{11}$, $\varepsilon_{01} = \varepsilon_{\mathrm{LD}}$, $\varepsilon_{12} = \varepsilon_{\mathrm{DP}}$, $\varepsilon_{02} = \varepsilon_{\mathrm{LP}}$, $\varepsilon_{22} = \varepsilon_{\mathrm{PP}}$. On the other hand, in the opposite case, $\varepsilon_{00} = \varepsilon_{\mathrm{DD}} = \varepsilon_{\mathrm{LL}} = \varepsilon_{11}$, $\varepsilon_{01} = \varepsilon_{\mathrm{DL}} (= \varepsilon_{\mathrm{LD}})$, $\varepsilon_{12} = \varepsilon_{\mathrm{LP}}$, $\varepsilon_{02} = \varepsilon_{\mathrm{DP}}$, $\varepsilon_{22} = \varepsilon_{\mathrm{PP}}$. Inserting these relations into eq (S7), we obtain expressions for the heat of dilution $q_{\mathrm{D,soln}\rightarrow\mathrm{L,dil}}$ in the former case, and that $q_{\mathrm{L,soln}\rightarrow\mathrm{D,dil}}$ in the latter case as

$$q_{\mathrm{D,soln}\rightarrow\mathrm{L,dil}} = \frac{z n_0 \left\{ {n_1}^2 \left(\varepsilon_{\mathrm{LD}} - \varepsilon_{\mathrm{DD}} \right) + n_1 n_2 \left(\varepsilon_{\mathrm{LD}} + \varepsilon_{\mathrm{LP}} - \varepsilon_{\mathrm{DD}} - \varepsilon_{\mathrm{DP}} \right) + {n_2}^2 \left[\varepsilon_{\mathrm{LP}} - \tfrac{1}{2}(\varepsilon_{\mathrm{DD}} + \varepsilon_{\mathrm{PP}}) \right] \right\}}{\left(n_0 + n_1 + n_2 \right)\left(n_1 + n_2 \right)} \tag{S8}$$

and

$$q_{\mathrm{L,soln}\to\mathrm{D,dil}}=\frac{zn_0\left\{n_1^{\,2}\left(\varepsilon_{\mathrm{LD}}-\varepsilon_{\mathrm{DD}}\right)+n_1n_2\left(\varepsilon_{\mathrm{LD}}+\varepsilon_{\mathrm{DP}}-\varepsilon_{\mathrm{DD}}-\varepsilon_{\mathrm{LP}}\right)+n_2^{\,2}\left[\varepsilon_{\mathrm{DP}}-\frac{1}{2}\left(\varepsilon_{\mathrm{DD}}+\varepsilon_{\mathrm{PP}}\right)\right]\right\}}{\left(n_0+n_1+n_2\right)\left(n_1+n_2\right)} \tag{S9}$$

Likewise, heats at diluted by the solvents, $q_{\mathrm{D,soln}\to\mathrm{D,dil}}$ and $q_{\mathrm{L,soln}\to\mathrm{L,dil}}$, are expressed by

$$q_{\mathrm{D,soln}\to\mathrm{D,dil}}=\frac{zn_0n_2^{\,2}\left[\varepsilon_{\mathrm{DP}}-\frac{1}{2}\left(\varepsilon_{\mathrm{DD}}+\varepsilon_{\mathrm{PP}}\right)\right]}{\left(n_0+n_1+n_2\right)\left(n_1+n_2\right)} \tag{S10}$$

and

$$q_{\mathrm{L,soln}\to\mathrm{L,dil}}=\frac{zn_0n_2^{\,2}\left[\varepsilon_{\mathrm{LP}}-\frac{1}{2}\left(\varepsilon_{\mathrm{DD}}+\varepsilon_{\mathrm{PP}}\right)\right]}{\left(n_0+n_1+n_2\right)\left(n_1+n_2\right)} \tag{S11}$$

Using eqs (S8) – (S11), the difference among the above four heats of dilution is given by

$$\begin{aligned}\left(q_{\mathrm{D,soln}\to\mathrm{L,dil}}-q_{\mathrm{D,soln}\to\mathrm{D,dil}}\right)-\left(q_{\mathrm{L,soln}\to\mathrm{D,dil}}-q_{\mathrm{L,soln}\to\mathrm{L,dil}}\right)&=\frac{2n_0n_2z\left(\varepsilon_{\mathrm{LP}}-\varepsilon_{\mathrm{DP}}\right)}{n_0+n_1+n_2}\\&\approx 2n_2z\left(\varepsilon_{\mathrm{LP}}-\varepsilon_{\mathrm{DP}}\right)\quad\left(n_0>>n_1+n_2\right)\end{aligned} \tag{S12}$$

When the structural unit of the polymer is changed from the segment (with same volume as the solvent) to the repeating unit, we should replace $n_2(\varepsilon_{\mathrm{LP}}-\varepsilon_{\mathrm{DP}})$ by the $n_{\mathrm{P}}(\varepsilon'_{\mathrm{LP}}-\varepsilon'_{\mathrm{DP}})$ where n_{P} is the number of the repeating units in the diluted solution, and $\varepsilon'_{\mathrm{LP}}$ and $\varepsilon'_{\mathrm{DP}}$ are the attractive potential energies per repeating unit. Finally, we obtain the following equation

$$\left(q_{\mathrm{D,soln}\to\mathrm{L,dil}}-q_{\mathrm{D,soln}\to\mathrm{D,dil}}\right)-\left(q_{\mathrm{L,soln}\to\mathrm{D,dil}}-q_{\mathrm{L,soln}\to\mathrm{L,dil}}\right)=2n_{\mathrm{p}}z\left(\varepsilon'_{\mathrm{LP}}-\varepsilon'_{\mathrm{DP}}\right) \tag{S13}$$

In the text, we discuss the relation between the heat of dilution and the intramolecular hydrogen binding between the neighboring glucose residues connected by the glucosidic linkage, of which internal rotation determines the local conformation of ATBC. However, the choice of the normal glucose residue as the repeating unit is inconvenient to discuss the above relation, because the glucosidic linkage, we are interested in, is not included in the repeating unit. We can escape this inconvenience by choosing the structural unit enclosed by the dotted ellipsoid in the following scheme as the repeating unit.

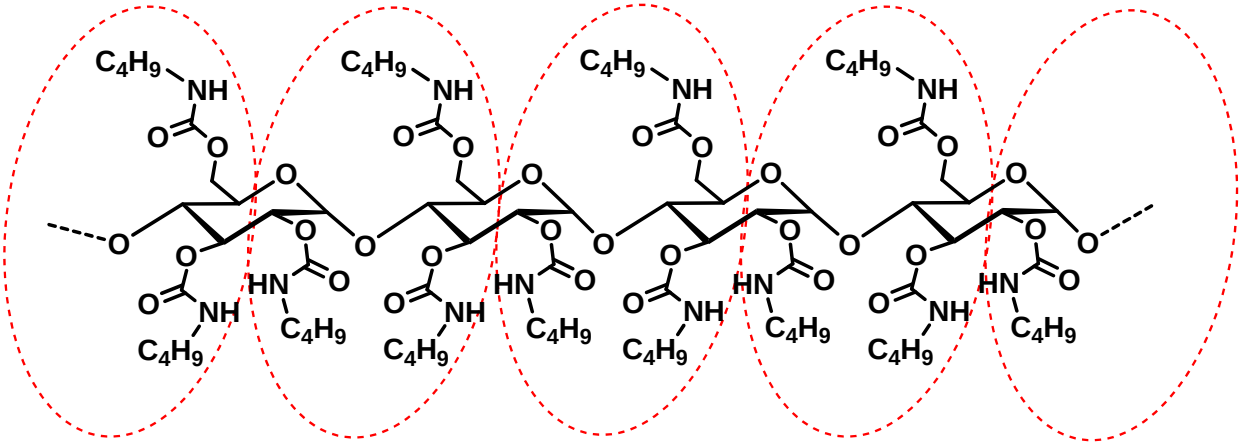

Fig. S3. Schematic representation of the repeating units in the lattice model.

References and Notes

1. I. Livsey, *J. Chem. Soc. Faraday. Trans. 2*, 1987, **83**, 1445-1452.
2. T. Konishi, T. Yoshizaki, T. Saito, Y. Einaga and H. Yamakawa, *Macromolecules*, 1990, **23**, 290-297.
3. O. Kratky and G. Porod, *Recl. Trau. Chim. Pays-Bas*, 1949, **68**, 1106.
4. M. L. Mansfield, *Macromolecules*, 1986, **19**, 854-859.
5. P. J. Flory, *Principles of Polymer Chemistry*, Cornell University Press, Ithaca, NY, USA, 1953.